

**Nonequilibrium hysteresis and Wien effect water dissociation at a bipolar membrane**D. T. Conroy,<sup>1</sup> R. V. Craster,<sup>2</sup> O. K. Matar,<sup>1</sup> L.-J. Cheng,<sup>3</sup> and H.-C. Chang<sup>3</sup><sup>1</sup>*Department of Chemical Engineering, Imperial College London, South Kensington Campus, London SW7 2AZ, United Kingdom*<sup>2</sup>*Department of Mathematics, Imperial College London, South Kensington Campus, London SW7 2AZ, United Kingdom*<sup>3</sup>*Department of Chemical and Biomolecular Engineering, University of Notre Dame, Notre Dame, Indiana 46556, USA*

(Received 1 March 2012; revised manuscript received 15 September 2012; published 6 November 2012)

As in electrochemical cyclic voltammetry, time-periodic reverse voltage bias across a bipolar membrane is shown to exhibit hysteresis due to transient effects. This is due to the incomplete depletion of mobile ions, at the junction between the membranes, within two adjoining polarized layers; the layer thickness depends on the applied voltage and the surface charge densities. Experiments show that the hysteresis consists of an Ohmic linear rise in the total current with respect to the voltage, followed by a decay of the current. A limiting current is established for a long period when all the mobile ions are depleted from the polarized layer. If the resulting high field within the two polarized layers is sufficiently large, water dissociation occurs to produce proton and hydroxyl traveling wave fronts which contribute to another large jump in the current. We use numerical simulation and asymptotic analysis to interpret the experimental results and to estimate the amplitude of the transient hysteresis and the water-dissociation current.

DOI: [10.1103/PhysRevE.86.056104](https://doi.org/10.1103/PhysRevE.86.056104)

PACS number(s): 47.61.Fg, 47.57.jd, 82.39.Wj

**I. INTRODUCTION**

Bipolar membranes formed by joining a cation and anion exchange membrane to form a p-n (boundary between a p-type and n-type material) junction are important for many industrial applications. For example, if reverse bias is applied across the bipolar membrane such that the mobile ions are depleted at the junction, the field at the junction can exceed 10 MV/cm such that water can be dissociated. The resulting proton and hydroxyl ions are then separated by the reverse bias into different membranes such that acidic and basic solutions are generated at the external boundaries of the bipolar membrane. If this can be achieved in a microfluidic chip, it would allow on-chip pH control for microreactors [1] or molecular separation [2], as demonstrated recently [3].

In this paper, we investigate a peculiar phenomenon first uncovered in a microfluidic bipolar membrane cured by photopolymerization [4]. When the reverse bias across the bipolar membrane is varied cyclically in time, a curious *I-V* hysteresis develops as in electrode cyclic voltammetry [4]. The amplitude of this hysteresis is scan rate dependent and disappears for very low scan rates. If the period is sufficiently long, a large current spike occurs due to water dissociation, quite analogous to the electron-transfer reaction spikes in cyclic voltammetry. Classical semiconductor theories for p-n junctions and Donnan theories for bipolar membranes are equilibrium theories that cannot describe such transient hysteresis [5,6]. For example, it is known that mobile ions within two thin boundary layers at the junction are depleted at equilibrium, thus producing two membrane regions with opposite net charge. It is known that these polarized layers are small, on the order of the Debye length, but are surface charge density and bias voltage dependent. It is also known that, since most of the voltage drop occurs within these two thin polarized layers, where the membrane conductivity vanishes, the field across these two polarized layers can exceed the threshold 10 MV/cm necessary to dissociate water due to the second Wien effect [7]. We extend such classical equilibrium theories

here to study the transient hysteretic response under cyclic or other reverse bias forcing.

Simons suggested a catalytic mechanism for water splitting [8–11], where water loses a proton to the amino surface group of an anion exchange membrane but the proton is soon released from the functional group, resulting in a net generation of both mobile hydroxyl and proton ions. Zabolotskii *et al.* [12] have recently observed that phosphoric acid group cation exchange membranes also intensely split water. If the catalytic step is fast, our kinetic model is still valid and one can simply change the activation energy of the field-dependent Arrhenius rate expression for the forward reaction to include this catalytic effect of surface protonation and deprotonation steps, as was done in an earlier report [5]. Our model can hence also capture catalyzed water-splitting mechanisms in terms of a bulk conversion rate, although we are not able to discern the various catalytic mechanisms that have been proposed. However, since different mechanisms are sensitive to different bivalent cation and amino acid concentrations [9], a more detailed version of our model which includes other reactants (including the surface groups) and a more complete reaction network will likely be able to discriminate against the different mechanisms. In this paper, however, we report a model that can capture the effective water splitting reaction, the resulting pH front propagation phenomena, and their “coarse” cyclic voltammetry signatures due to overall pH generation without the finer features unique to the specific catalytic mechanism. We quantitatively characterize several regimes in the hysteresis and relate them to diffusive depletion dynamics and pH traveling shocks by analyzing the appropriate volume averaged Poisson and Nernst-Planck equations, which are time-dependent (and therefore nonequilibrium) extensions of the classical Donnan theory.

The plan of the paper is as follows: we begin by formulating the problem in Sec. II, identifying key nondimensional groups and reducing the model to a form that encapsulates the essential physics in Sec. II B. Section III gives an extensive experimental

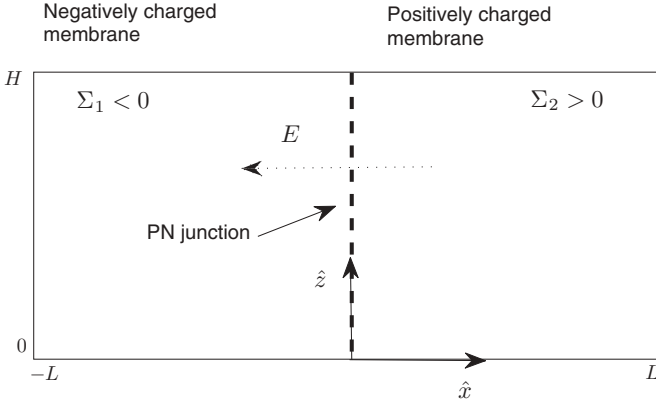


FIG. 1. Diagram of a bipolar membrane composed of a negatively charged membrane (denoted 1) and a positively charged membrane (denoted 2) joined at  $\hat{x} = 0$  and  $\hat{z} = 0$  to form a p-n junction. Two electrolytes,  $\hat{C}_a^{(\pm)}$  and  $\hat{C}_b^{(\pm)}$ , fill the pore space, and a time-dependent electric field  $\hat{\mathbf{E}}(\hat{t})$  is applied normal to the junction.

study of the hysteresis phenomenon and follows that with a numerical study of the model identified earlier. Finally asymptotic techniques extract further details with concluding remarks providing closure in Sec. IV.

## II. GOVERNING EQUATIONS

We consider the setup shown in Fig. 1, where two ion exchange membranes of length  $L$  and depth  $H$  are joined at a junction located at  $\hat{x} = 0$  and have charges  $\Sigma_1$  ( $\hat{x} < 0$ ) and  $\Sigma_2$  ( $\hat{x} > 0$ ). Generally the bipolar membranes are held in an electrolyte bath [3] with a salt species  $\hat{C}_b^{(+)}, \hat{C}_b^{(-)}$  and water of concentration  $\hat{C}_a$  that is assumed to be constant. The salt is added to the system to maintain electroneutrality so that the ion charges balance the membrane surface charges at equilibrium.

To this system an electric field  $\hat{\mathbf{E}}$  is applied across the bipolar membrane causing the water to dissociate into cationic and ionic species  $\hat{C}_a^{(+)}, \hat{C}_a^{(-)}$ . It is also common to assume that the electric field is irrotational, which permits its expression in terms of a voltage potential  $\hat{\phi}$  through the relationship  $\hat{\mathbf{E}} = -\nabla\hat{\phi}$ . Since the electric field is a maximum at the p-n junction, most of the dissociated water ions are produced in a thin region that is on the order of the Debye length. In this thin layer ions are forced out by ion migration, forming an ion depletion region. A mathematical model describing the system will include the transport of ions with a water dissociation reaction, which is coupled to an equation for the charge dependent voltage potential, and the flow of bulk fluid due to stresses in the system.

The flow of bulk fluid is governed by Darcy's law with conservation of mass [13]

$$\nabla \hat{P} = -\frac{\mu}{\Pi} \hat{\mathbf{u}} + \hat{\rho}^e \hat{\mathbf{E}}, \quad (1)$$

$$\nabla \cdot \hat{\mathbf{u}} = 0, \quad (2)$$

where, here,  $\hat{\mathbf{u}}$  is the filtration rate,  $\hat{P}$  is the pressure,  $\mu$  is the viscosity,  $\Pi$  is the permeability, and  $\hat{\rho}^e$  is the volumetric

charge density defined as

$$\hat{\rho}^e = F(\hat{C}_a^{(+)} - \hat{C}_a^{(-)} + \hat{C}_b^{(+)} - \hat{C}_b^{(-)}). \quad (3)$$

Here  $F = N_A e$  is the Faraday constant,  $e$  is the charge on an electron, and  $N_A$  is Avagadro's number. The term  $\hat{\rho}^e \hat{\mathbf{E}}$  on the right-hand side of (1) is a Maxwell pressure that allows for fluid motion by the presence of charged species in an electric field. The ionic concentrations evolve according to the Nernst-Planck equations [14]

$$\begin{aligned} n \frac{\partial \hat{C}_a^{(\pm)}}{\partial \hat{t}} + \hat{\mathbf{u}} \cdot \nabla \hat{C}_a^{(\pm)} \\ = \omega_a^{(\pm)} k_B T \nabla \cdot \left( \pm \frac{e}{k_B T} \hat{C}_a^{(\pm)} \nabla \hat{\phi} + \nabla \hat{C}_a^{(\pm)} \right) \\ + (m_f \hat{C}_a - m_r \hat{C}_a^{(+)} \hat{C}_a^{(-)}), \end{aligned} \quad (4)$$

$$\begin{aligned} n \frac{\partial \hat{C}_b^{(\pm)}}{\partial \hat{t}} + \hat{\mathbf{u}} \cdot \nabla \hat{C}_b^{(\pm)} \\ = \omega_b^{(+)} k_B T \nabla \cdot \left( \pm \frac{e}{k_B T} \hat{C}_b^{(\pm)} \nabla \hat{\phi} + \nabla \hat{C}_b^{(\pm)} \right), \end{aligned} \quad (5)$$

where  $n$ ,  $k_B$ ,  $T$ , and  $\omega_{a,b}^{(\pm)}$  are the porosity, Boltzmann's constant, absolute temperature, and mobility of the species, respectively. Equations (4) and (5) represent four equations with the superscripts  $(\pm)$  representing the cations and anions respectively.

In these equations the first term on the right-hand side represents ion transport by ion migration and molecular diffusion. The last term on the right-hand side of (4) is the reaction rate that arises from a kinetic model of the dissociation and association of the ions, with rates  $m_f$  and  $m_r$ , respectively.  $m_f$  is a function of the potential from the Wien effect [7]:  $m_f = k_a [1 + \epsilon_r (e/k_B T) |\hat{\phi}_x|]$  (where  $|\hat{\phi}_x|$  is the absolute value), with constants  $k_a$  and  $\epsilon_r$ . Here  $\epsilon_r e/k_B T$  is the dissociation rate constant in units of m/V. In this expression  $\epsilon_r$  is a modified water dissociation rate constant obtained from [7] but should not be confused with the notation in their paper.

The voltage potential is governed by the Poisson-Boltzmann equation

$$\epsilon_0 \epsilon \nabla^2 \hat{\phi} = -\hat{\rho}^e - F[\Sigma_1 H(-\hat{x}) + \Sigma_2 H(\hat{x})], \quad (6)$$

where  $\epsilon_0$  is the permittivity of free space,  $\epsilon$  is the relative permittivity, and  $H(\hat{x})$  is a Heaviside step function, and we include surface charges in the volume averaged equation to obtain an effective homogeneous equation [15,16].

The usual no-flux and no-penetration conditions apply at the walls of the membrane:  $\hat{\phi}_{\hat{z}}(\pm H, \hat{x}, \hat{t}) = 0$ ,  $\hat{C}_{a,b\hat{x}}^{(\pm)}(\pm H, \hat{x}, \hat{t}) = 0$ , and  $\hat{u}(\pm H, \hat{x}, \hat{t}) = 0$ , where  $\hat{z}$  subscripts denote partial derivatives with respect to  $\hat{z}$ . At the ends of the domain we fix the potential,  $\hat{\phi}(\hat{z}, \pm L, \hat{t}) = \pm \beta(\hat{t})L$  (where  $\beta$  is a given function of time), and the horizontal concentration gradients to be zero,  $\hat{C}_{a,b\hat{x}}^{(\pm)}(\hat{z}, \pm L, \hat{t}) = 0$ . The latter condition is appropriate if the reservoir joining the boundaries has a uniform concentration or the channel is very long with ion migration dominating molecular diffusion, as considered here. Initially, the concentration of the products is set to the equilibrium value in the absence of an electric field,  $\hat{C}_a^{(\pm)}(\hat{z}, \hat{x}, 0) = C_{eq} = \sqrt{m_f \hat{C}_a / m_r}$ , obtained from Eq. (4), and

the salt concentration is set to achieve electroneutrality:

$$\hat{C}_b^{(+)} = (|\Sigma_1| + \hat{C}_b^{(-)}(-L))H(-\hat{x}) + C_b^{(+)}(L)H(\hat{x}), \quad (7)$$

$$\hat{C}_b^{(-)} = \hat{C}_b^{(-)}(-L)H(-\hat{x}) + (|\Sigma_2| + \hat{C}_b^{(+)}(L))H(\hat{x}). \quad (8)$$

The condition on the salt is equivalent to the Donnan equilibrium relationships. In our case we are investigating large membrane charges relative to the bathing electrolyte so the initial conditions reduce to  $\hat{C}_b^{(-)} = |\Sigma_2|H(\hat{x})$  and  $\hat{C}_b^{(+)} = |\Sigma_1|H(-\hat{x})$ .

### A. Nondimensionalization

To make sense of the equations, and extract the essential physics, we now nondimensionalize with the aim of arriving at a simplified set of equations. We scale  $\hat{x}$  on the half-length of the domain  $L$ ,  $\hat{z}$  on the depth  $H$ , the potential  $\hat{\phi}$  on the maximum potential  $\phi_c = \max(\beta)L$ , time on the diffusive scale  $nL^2/k_B T \omega_b^+$ , the concentrations on the membrane charge  $|\Sigma_1|$ , the horizontal filtration rate  $\hat{u}$  on  $\Pi|\Sigma_1|k_B T F/\mu e L$ , the pressure  $P$  on  $|\Sigma_1|k_B T F/e$ , and the vertical filtration rate  $\hat{w}$  on  $(H/L)\Pi|\Sigma_1|k_B T F/\mu e L$ . From here we define variables with hats as dimensional and variables without hats as dimensionless. For Darcy's law and continuity, the equations are

$$\frac{\partial P}{\partial x} = -u - \psi \rho^e \frac{\partial \phi}{\partial x}, \quad (9)$$

$$\frac{\partial P}{\partial z} = -\frac{H^2}{L^2} w - \psi \rho^e \frac{\partial \phi}{\partial z}, \quad (10)$$

$$\frac{\partial u}{\partial x} + \frac{\partial w}{\partial z} = 0, \quad (11)$$

where the dimensionless group  $\psi = \phi_c e/k_B T$  represents the strength of the electric field. The ion transport equations are

$$\begin{aligned} & \frac{\partial C_a^{(\pm)}}{\partial t} + \text{Pe} \left( u \frac{\partial C_a^{(\pm)}}{\partial x} + w \frac{\partial C_a^{(\pm)}}{\partial z} \right) \\ &= \alpha_a^{(\pm)} \frac{\partial}{\partial x} \left( \pm \psi C_a^{(\pm)} \frac{\partial \phi}{\partial x} + \frac{\partial C_a^{(\pm)}}{\partial x} \right) \\ &+ \alpha_a^{(\pm)} \frac{L^2}{H^2} \frac{\partial}{\partial z} \left( \pm \psi C_a^{(\pm)} \frac{\partial \phi}{\partial z} + \frac{\partial C_a^{(\pm)}}{\partial z} \right) + \text{Da} R, \end{aligned} \quad (12)$$

for the dissociated water ions, and

$$\begin{aligned} & \frac{\partial C_b^{(\pm)}}{\partial t} + \text{Pe} \left( u \frac{\partial C_b^{(\pm)}}{\partial x} + w \frac{\partial C_b^{(\pm)}}{\partial z} \right) \\ &= \alpha_b^{(\pm)} \frac{\partial}{\partial x} \left( \pm \psi C_b^{(\pm)} \frac{\partial \phi}{\partial x} + \frac{\partial C_b^{(\pm)}}{\partial x} \right) \\ &+ \alpha_b^{(\pm)} \frac{L^2}{H^2} \frac{\partial}{\partial z} \left( \pm \psi C_b^{(\pm)} \frac{\partial \phi}{\partial z} + \frac{\partial C_b^{(\pm)}}{\partial z} \right), \end{aligned} \quad (13)$$

for the salt, where the dimensionless groups appearing above are the mobility ratios, Peclet number, and Damkholer number:

$$\alpha_{a,b} = \frac{\omega_{a,b}^{(\pm)}}{\omega_b^{(+)}}, \quad \text{Pe} = \frac{\Pi F |\Sigma_1|}{\mu e \omega_b^{(+)}}, \quad \text{Da} = \frac{L k_a C_a \epsilon_r}{k_B T \omega_b^{(+)} |\Sigma_1|}. \quad (14)$$

Here the Peclet and Damkholer numbers represent a ratio of convection to diffusion of ions and water dissociation rate to

ion diffusion, respectively. Also the mobility ratios, relating the mobility of cations to anions, is a small parameter. The reaction rate is expressed as

$$R = (\psi |\phi_x| + \bar{\epsilon}_r^{-1} - \bar{\epsilon}_r^{-1} \bar{m}^{-1} C_a^{(+)} C_a^{(-)}), \quad (15)$$

where the Arrhenius dependence of the water-splitting reaction, possibly with Simons' catalytic step [5], has been linearized by assuming weak activation. The constants are defined as  $\bar{m} = k_a \hat{C}_a / (|\Sigma_1|^2 m_r)$  and  $\bar{\epsilon}_r = \epsilon_r / L$ . The second Wien effect is represented by the term  $\psi |\phi_x|$  and the other terms represent the equilibrium reaction. For large  $\text{Da}$  and small  $\psi$ , the concentrations are at the equilibrium values  $C_a^{(\pm)} = \sqrt{\bar{m}}$ . The potential is determined from the Poisson-Boltzmann equations, Eq. (6), expressed as

$$\frac{\partial^2 \phi}{\partial x^2} + \frac{L^2}{H^2} \frac{\partial^2 \phi}{\partial z^2} = -\chi^2 \rho^e - \chi^2 \bar{\Sigma}, \quad (16)$$

$$\rho^e = (C_a^{(+)} - C_a^{(-)} + C_b^{(+)} - C_b^{(-)}), \quad (17)$$

with the dimensionless groups:

$$\bar{\Sigma}_i = \frac{\Sigma_i}{|\Sigma_1|}, \quad \chi^2 = \psi^{-1} \frac{F L^2 |\Sigma_1| e}{\epsilon \epsilon_0 k_B T}, \quad (18)$$

for the charge ratio, with  $\bar{\Sigma} = -H(-x) + \bar{\Sigma}_2 H(x)$ , and the inverse Debye length, respectively. The dimensionless inverse Debye length  $\chi$  represents the ratio of the ion depletion width at the junction to the channel length.

The dimensionless boundary conditions are  $\phi_z(\pm H, x, t) = 0$ ,  $C_{a,bz}^{(\pm)}(\pm H, x, t) = 0$ , and  $u(\pm H, x, t) = 0$  at the upper and lower walls and  $\phi(z, \pm L, t) = \pm \bar{\beta}$  (where  $\bar{\beta} = \beta L / \phi_c$ ) and  $C_{a,bx}^{(\pm)}(z, \pm L, t) = 0$  at the ends. Initially,  $C_a^{(\pm)} = \sqrt{\bar{m}}$ ,  $C_b^{(-)} = |\bar{\Sigma}_2| H(x)$  and  $C_b^{(+)} = H(-x)$ .

### B. One-dimensional model

The next stage in the reduction is to assume that the membrane is long and thin so that a small parameter  $\epsilon$  is introduced:  $\epsilon = H/L \ll 1$ . This assumption is valid in many cases, including the experiments presented in this paper. We rewrite the potential by introducing a perturbation potential  $\phi'$  such that  $\phi = \phi' + \bar{\beta}(t)x$ . At leading order  $P_z = 0$ ,  $\phi'_z = 0$ ,  $C_{iz}^{(\pm)} = 0$ , and  $u = u(x, t)$ . Therefore we expand as  $\phi' = \phi'_0(x, t) + \epsilon^2 \phi'_1(z, x, t)$  and  $C_{iz}^{(\pm)} = C_{i0z}^{(\pm)}(x, t) + \epsilon^2 C_{i1z}^{(\pm)}(z, x, t)$  and integrate the equations across the channel to obtain depth-averaged equations:

$$\frac{\partial P}{\partial x} = -u - \psi \rho^e \frac{\partial \phi}{\partial x}, \quad (19)$$

$$\frac{\partial^2 \phi'}{\partial x^2} = -\chi^2 (C_a^{(+)} - C_a^{(-)} + C_b^{(+)} - C_b^{(-)} + \bar{\Sigma}), \quad (20)$$

for Darcy's law and the Poisson-Boltzmann equation, respectively. For the dissociated water ions the equation reduces to

$$\begin{aligned} & \frac{\partial C_a^{(\pm)}}{\partial t} + \text{Pe} \frac{\partial C_a^{(\pm)}}{\partial x} u \\ &= \alpha_a^{(\pm)} \frac{\partial}{\partial x} \left( \pm \psi C_a^{(\pm)} \left( \frac{\partial \phi'}{\partial x} + \bar{\beta}(t) \right) + \frac{\partial C_a^{(\pm)}}{\partial x} \right) + \text{Da} R, \end{aligned} \quad (21)$$

and for the salt to

$$\begin{aligned} \frac{\partial C_b^{(\pm)}}{\partial t} + \text{Pe} \frac{\partial C_b^{(\pm)}}{\partial x} u \\ = \alpha_b^{(\pm)} \frac{\partial}{\partial x} \left( \pm \psi C_b^{(\pm)} \left( \frac{\partial \phi'}{\partial x} + \bar{\beta}(t) \right) + \frac{\partial C_b^{(\pm)}}{\partial x} \right), \quad (22) \end{aligned}$$

where the subscripts have been dropped. Further, we eliminate the convective term for  $\text{Pe} \ll 1$  or force  $\partial P / \partial x = -\psi \rho^e \partial \phi / \partial x$ , so that we can ignore hydrodynamic effects as done by many authors [3,17]. Ignoring hydrodynamic effects is also consistent with our previous assumption of a constant water concentration so that junction drying is not a problem. The boundary condition on the perturbed potential is now is  $\phi'(z, \pm L, t) = 0$ , and the others are the same as before.

In addition we define ion fluxes as follows:  $J_a^{(+)} / \alpha_a^{(+)} = \psi C_a^{(+)} (\bar{\beta} + \phi'_x) + C_{ax}^{(+)}$  and  $J_a^{(-)} / \alpha_a^{(-)} = -\psi C_a^{(-)} (\bar{\beta} + \phi'_x) + C_{ax}^{(-)}$ , and from these expressions the dimensionless current is  $I = -(J_a^{(+)} - J_a^{(-)} + J_b^{(+)} - J_b^{(-)})$  with the negative sign added because of the way we define the fluxes. The current will be useful in Sec. III, where comparisons are made between the experimental and numerical results.

### III. RESULTS

Given the one-dimensional model we are now in a position to generate simulations of hysteresis and compare them qualitatively with experiments.

We solve Eqs. (20) to (22) numerically using the boundary and initial conditions with variations in the parameters  $\chi$ ,  $\psi$ ,  $\bar{\beta}$ ,  $\text{Da}$ ,  $\bar{m}$ ,  $\bar{\epsilon}_r$ , and  $\bar{\Sigma}_2$ . Given the rich parameter space it is worth noting specifically what they each represent:  $\chi^2$  is the inverse Debye length,  $\psi$  is the strength of the electric field,  $\bar{\beta}$  is a scaled electric field,  $\text{Da}$  is the Damkohler number relating the reaction rate to the species diffusion,  $\bar{m}$  is related to the equilibrium concentration without an electric field,  $\bar{\epsilon}_r$  is the strength of the Wien effect, and  $\bar{\Sigma}_2$  is the membrane charge of region 2 ( $x \geq 0$ ) relative to region 1.

In the simulations we use estimates of the size of the dimensionless groups using data from the literature [7]:  $\epsilon_r = 1.38 \times 10^{-8}$  m at room temperature,  $m_r = 1.5 \times 10^{14}$  cm<sup>3</sup> mol<sup>-1</sup> s<sup>-1</sup>, and  $k_a = 2 \times 10^{-5}$  s<sup>-1</sup>. In addition, we take  $k_B T / e = 25$  mV and  $k_B T \omega_a^{(+)} \sim 1 \times 10^{-9}$  m<sup>2</sup>/s. Assuming experimental conditions with  $|\Sigma_1| \sim 1$  mol m<sup>-3</sup> to  $2 \times 10^3$  mol m<sup>-3</sup>,  $\phi_c \sim 1$  to 100 V, and  $L \sim 1 \times 10^{-4}$  to  $1 \times 10^{-3}$  m, we get the following estimates for the dimensionless groups concerning the reaction:  $\text{Da} \ll 1$ ,  $\bar{m} \ll 1$ , and  $\psi \gg 1$ . Also, in our experiments the salt mobilities are approximately the same and small compared to the hydrogen ions so we can define:  $\alpha_b^{(+)} = \alpha_b^{(-)} = 1$  and  $\alpha_a^{(+)} \gg 1$ .

A useful estimate for the performance of the system is the thermodynamic yield, which allows us to explicitly estimate how much we have shifted the yield or conversion beyond the thermodynamic limit. The thermodynamic yield is defined as the product concentration, using the rates at the external field before depletion, that is at thermodynamic equilibrium with the initial reactant concentration. This is defined as

$$C_a^{(+)} \sim \sqrt{\bar{m} + \bar{m} \bar{\epsilon}_r \psi |\bar{\beta}|}, \quad (23)$$

and the nonequilibrium concentration of hydrogen ions,  $C_a^{(+)}$ , relative to the thermodynamic yield is just  $1 / \sqrt{\bar{m} + \bar{m} \bar{\epsilon}_r \psi |\bar{\beta}|}$ . Since we are removing products, we expect the bipolar membrane to do better than the thermodynamic yield at the enhanced field. From the concentration the current, with no salt ions and membrane charges, is  $I_{\text{therm}} = \psi \bar{\beta} (\alpha_a^{(+)} + \alpha_a^{(-)}) \sqrt{\bar{m} + \bar{m} \bar{\epsilon}_r \psi |\bar{\beta}|}$ .

#### A. Hysteresis

Before embarking upon numerical simulations, we first report a more extensive experimental study of the hysteresis phenomenon observed in [3,4,18] with piecewise linear voltage scans. This is done by applying a ramp function in time as follows:  $\bar{\beta} = (2t/t_p)$  ( $0 \leq t \leq t_p/2$ ) and  $\bar{\beta} = 1 - (t - t_p/2)/(t_p - t_p/2)$  ( $t_p/2 \leq t \leq t_p$ ), where  $t_p$  is the scanning rate. Below we present some experimental results and numerical solutions.

#### 1. Experiments

Here we show the pronounced hysteresis effect that is observed in the  $I$ - $V$  characteristics of a polymeric bipolar membrane. Manufactured by photopolymerization of a negatively charged poly(2-acrylamido-2-methyl-1-propanesulfonic acid) (pAMPS) layer as a cation exchange membrane on the right-hand side and a positively charged poly(diallyldimethylammonium chloride) (pDADMAC) layer as an anion exchange membrane on the left-hand side, bridging two microfluidic channels, the bipolar membrane containing a 2M fixed charge concentration was precisely defined to be 500  $\mu\text{m}$  long in each side by photolithography in a 20- $\mu\text{m}$ -thick microfluidic channel: The materials and fabrication procedures were detailed in [4]. The  $I$ - $V$  characteristics were measured by an HP 4140 pA meter using a DC voltage source through a pair of Pt electrodes.

The bipolar membrane exhibits unique hysteresis features under reverse bias at which the cathode is connected to the cationic side. Figure 2(a) shows the cyclic  $I$ - $V$  curves measured in a 10 mM KCl solution with three different voltage sweep rates, 0.02, 0.1, and 0.4 V/s. The voltage sweeps linearly back and forth between 0 and  $-2.5$ V. It has been reported in our previous work [4] that the hysteresis loop results from the transient response of the ion depletion at the membrane junction. As shown in Fig. 2(a), when the voltage is swept from zero to negative values, the current intensity increases linearly in the beginning, then drops precipitously after a turning point and finally reaches a saturation level. With a reverse voltage sweep from negative to zero, the current decreases monotonically at a low conductance. To further understand the transient response of the bipolar membrane, here we investigate the effect of the voltage scan rate on the hysteresis phenomenon. It can be found that with a higher voltage sweep rate the device has its turning point at greater current intensity and reaches saturation at a larger voltage, yielding a broader hysteresis loop. The time evolution of current in Fig. 2 also shows that the high voltage scan rate brings the system far away from equilibrium, resulting in large maximum current (the peaks) and saturation current,

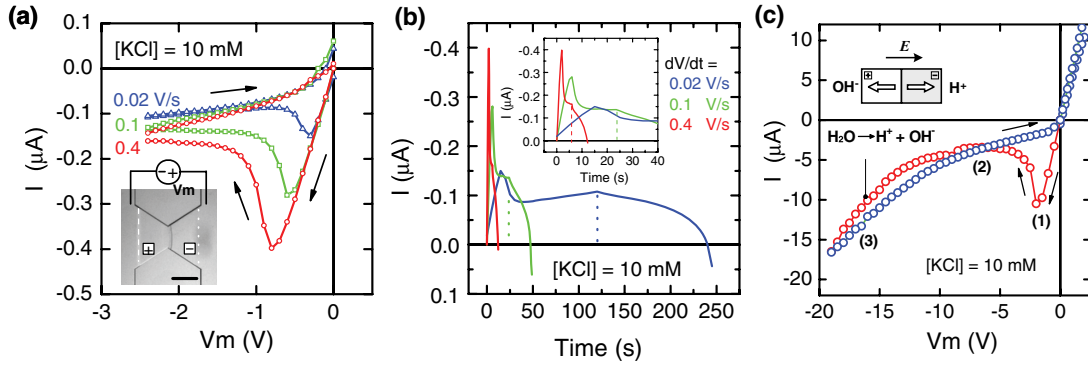


FIG. 2. (Color) (a) Measured  $I$ - $V$  hysteresis of a bipolar membrane under various voltage sweep rates. Linear voltage sweeps were applied back and forth between 0 and  $-2.5$  V. The inset shows a bipolar membrane device fabricated by photopolymerization in a microfluidic channel. Positive and negative symbols indicate the fixed charges in pADMAC and pAMPS membranes, respectively. The scale bar is  $300 \mu\text{m}$ . (b) Time evolution of current at different voltage sweep rates. The dashed lines indicate the times the voltage scan reverses for different scan rates. The inset shows the detail within 45 sec. (c) For large periods, a large increase in the negative current is observed, where the numbers 1, 2, and 3 represent the hysteresis, saturation, and water splitting regimes, respectively (image reproduced from [4]).

i.e., the current level around the region indicated by the dashed line where the voltage scan starts reversing, as shown Fig. 2(b). Based on the trend observed in the experiment, the hysteresis loop is expected to disappear when the device is measured under an infinitely slow sweep rate in which the system remains in quasistatic equilibrium throughout the measurement.

For larger reverse biases, shown in Fig. 2(c), the system is in a water splitting regime with the production of protons and hydroxide ions creating an elevated ion current. The size of the current in this regime is a function of the water dissociation rate and exhibits an increase when the voltage bias ramps up and a decrease when the dissociation rate is alleviated by a voltage scan from negative to zero.

2. Numerical solution

We now proceed to simulate the hysteresis numerically. The current against potential and concentrations are plotted in Figs. 3 to 5 for different scanning rates  $t_p$ , corresponding to one cycle, and different  $Da$ . For the early stages, the evolution of the curve is due primarily to the salt ions since the concentration of ions from water dissociation is negligible. As the potential is swept from zero to negative values, the current amplitude increases linearly in the negative direction since the electric field is due to just  $\bar{\beta}$ . When the potential is sufficiently large an electroneutral region forms around the junction, causing the electric field to increase and the current to decrease. As the potential continues to be swept towards negative unity the width of the electroneutral region surrounding the junction continues to grow and the concentration of  $C_a^{(\pm)}$  increases. At this point, water dissociation becomes faster and the membrane is in the water-splitting regime.

When  $\bar{\beta} = 1$ , the potential is swept back towards zero and a hysteresis curve develops that increases in size as the period decreases. At this point the salt has been swept away from the measuring point so the current is due to only the dissociated water ions. As the potential decreases from negative to zero the

ion migration strength decreases and the electroneutral region thins.

We get hysteresis curves regardless of water dissociation, as shown in Fig. 3(b). The effect of water dissociation is to increase the current for large potentials. In these numerical solutions the limiting current, defined as the current without water dissociation and infinitely long scans, is zero because the co-ion concentration at the boundaries is taken to be small. The signature of the Wien effect is illustrated more clearly by setting  $\psi|\phi_x| = 0$  in Eq. (15), as shown in Fig. 4. For  $Da \ll 1$  the current-voltage curve, without the Wien effect, collapses onto the  $Da = 0$  case with the Wien effect turned on. In the absence of the Wien effect, Fig. 4, it is only for extremely large values of  $Da$  that the current shows a noticeable increase at high voltage. Clearly the Wien effect dominates the current-voltage characteristic in the water splitting region but not in the beginning stages for small  $\phi$ .

3. Minimum current

From both the experiments and numerical solutions, we find that the amplitude of the hysteresis can be characterized by a minimum in the current, seen in Figs. 2 and 3, at low voltage when the mobile ion depletion is incomplete and the field at the junction is not sufficiently high to dissociate water. The minimum current occurs at a time when the ion depletion region first forms, causing the electric field far from the junction,  $\phi'_x \sim O(\bar{\beta}t)$ . At early times we can make the following approximation,  $\phi'_x/\bar{\beta}t \ll 1$ , and expand about this small value. Since this point on the curve is not in the water splitting regime (the electric field at the junction is small), we can ignore the water and investigate the model associated with the ion transport of salt species. In addition, the current can be approximated as  $I = -\psi \bar{\beta}(t)[\phi'_x/\bar{\beta}(t) + 1]$ , since diffusion is small far from the junction. The traveling wave speed of the salt ions is then time dependent and equal to  $s_b^{(\pm)} = I$ . Considering only the left-hand membrane, we can ignore the negative ions and solve the following

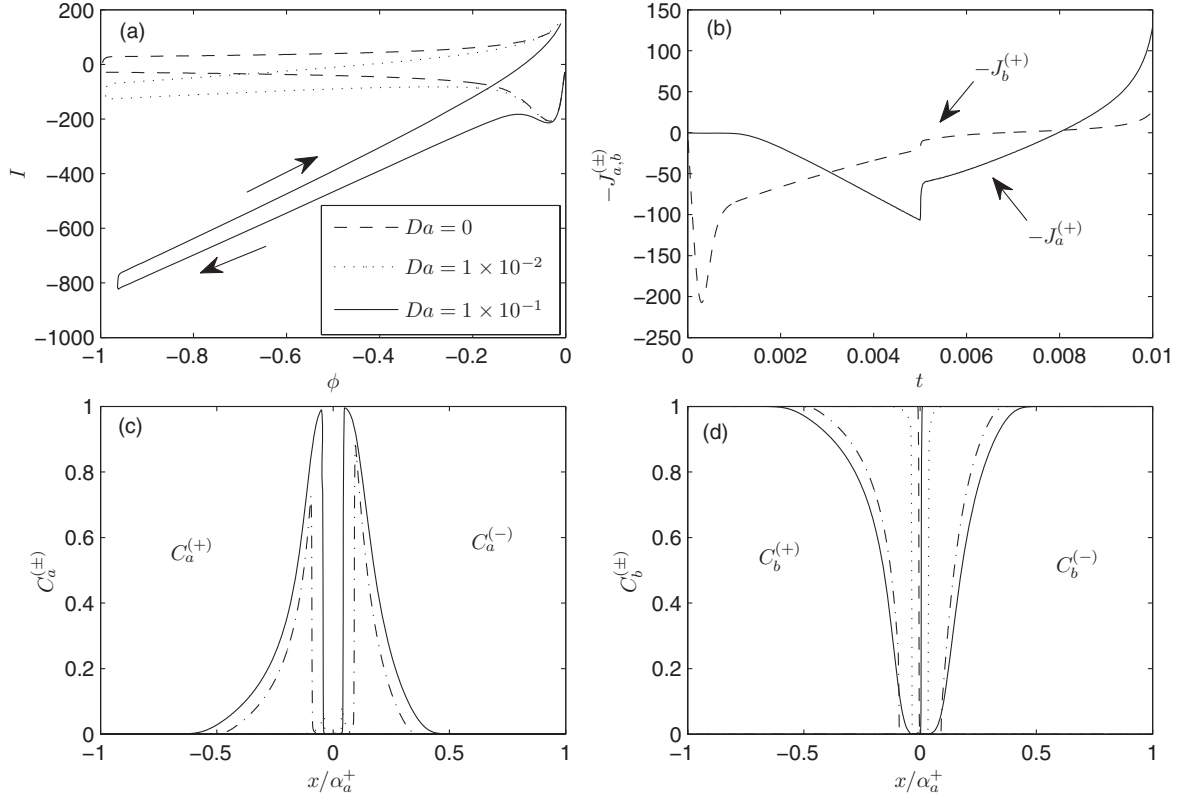


FIG. 3. (Top panels) Current against potential  $\phi$ , and ion flux against time for different values of  $Da$ . Also, the measuring point is at  $x = -0.35$  and the arrows indicate the direction of time. (Lower panels) Concentrations at the minimum current  $\phi = -0.034$  (dashed line),  $-0.2$  (dotted line and voltage ramping up),  $-1$  (dashed-dotted line), and  $-0.2$  (solid line and voltage ramping down) and the species flux as a function of time. The applied electric field  $\bar{\beta}$  varies by a ramp function given here as  $\bar{\beta} = (2t/t_p)$  ( $0 \leq t \leq t_p/2$ ) and  $\bar{\beta} = 1 - (t - t_p/2)/(t_p - t_p/2)$  ( $t_p/2 \leq t \leq t_p$ ). Here  $\alpha_a^{(+)} = 3$ ,  $\alpha_a^{(-)} = 2$ ,  $\bar{m} = 1 \times 10^{-6}$ ,  $Da = 1 \times 10^{-2}$  (upper right-hand and lower panels only),  $t_p = 0.01$ ,  $\epsilon = 1 \times 10^{-2}$ ,  $\chi = 5$ ,  $\bar{\Sigma}_2 = 1$ , and  $\psi = 5 \times 10^3$ .

equations:

$$\frac{\partial^2 \phi'}{\partial x^2} = -\chi^2 (C_b^{(+)} - 1), \quad (24)$$

$$\frac{\partial C_b^{(+)}}{\partial t} = \frac{\partial}{\partial x} \left( \psi \bar{\beta}(t) C_b^{(+)} (O(\delta) + 1) + \frac{\partial C_b^{(+)}}{\partial x} \right), \quad (25)$$

with  $\phi'(0, t) = 0$  since the membrane charges have the same magnitude and  $\delta$  is a small parameter. From here on, we only look at the solution for negative potentials (in this case  $\bar{\beta} = 2t/t_p$ ) since concentration of salt ions at the junction makes a solution more difficult to obtain in closed form.

Assuming that the diffusion of ions is small (true provided  $\psi \gg 1$ ), the solution is  $C_b^{(+)} = H(-\xi)$  with the characteristic coordinate  $\xi = x + \psi \int_0^t \bar{\beta} dt$ . Integrating Poisson's equation [Eq. (24)] twice, the potential is  $\phi'/\chi^2 = \xi^2 H(\xi)/2 - (1+x)(\psi \int \bar{\beta} dt)^2/2$ . The current at small voltage is then to leading order

$$I = -\psi \left( \bar{\beta} - \frac{\chi^2 \psi^2}{2} \left( \int \bar{\beta} dt \right)^2 \right). \quad (26)$$

We hence see that the low-voltage current first decays linearly with respect to voltage in an Ohmic manner, followed by a rise from a minimum for a linear voltage scan. Other ramping voltage functions would produce a different rise in the  $I$ - $V$  curve.

For the linear ramp at a small voltage of  $\bar{\beta} = 2t/t_p$ , where  $t_p$  is the final time, the minimum current can be estimated by setting  $dI/dt = 0$  to yield

$$I_{\min} = -\psi \left( \left( \frac{8}{\chi^2 \psi^2} \right)^{1/3} - \frac{1}{2} \chi^2 \psi^2 \left( \frac{1}{\chi^2 \psi^2} \right)^{4/3} \right) t_p^{-2/3}. \quad (27)$$

A plot comparing the asymptotic solution to the numerical one is shown in Fig. 5 along with the ion concentrations at different points along the hysteresis curve. In panel (a), the current initially follows the curve  $I \sim -\psi \bar{\beta}$ , but as the ion free region at the junction opens up,  $\phi'_x$  becomes significantly large to decrease the magnitude of the current. Our asymptotic solution is able to capture the approximate point where the current turns around by solving for the potential with the salt being flushed out of the junction. The asymptotic solution does a good job in approximating the trend for  $I_{\min}$  as a function of  $t_p$  (the inverse of the rate of voltage change), showing the slope of  $t_p^{-2/3}$ .

In the limit  $t_p \gg 1$  and  $Da \ll 1$ , the system approaches the equilibrium limiting current. Here an ion-free region will form near the junction and from the initial conditions, positive salt ions will be exclusively on the left-hand and negative salt ions on the right-hand membrane. This configuration yields

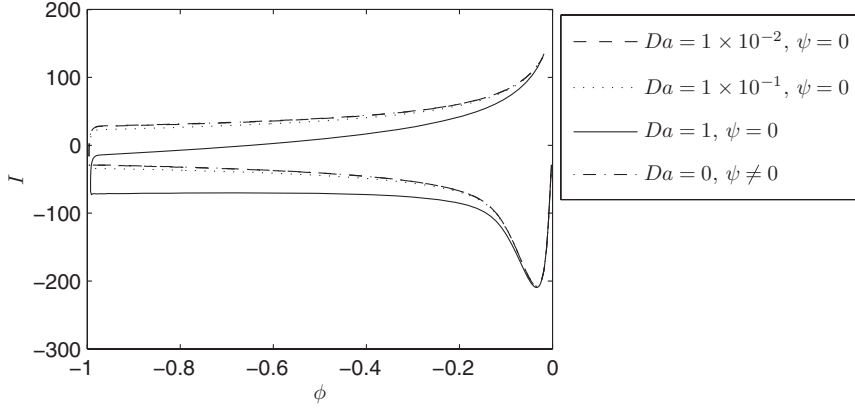


FIG. 4. Current against potential  $\phi$ , showing the solution for variations in  $Da$ :  $1 \times 10^{-2}$  (dashed line),  $1 \times 10^{-1}$  (dotted line), and 1 (solid line) with the Wien effect in Eq. (15) turned off by effectively setting  $\psi = 0$ . A solution for  $Da = 0$  and  $\psi \neq 0$  (dashed-dotted line) in Eq. (15) is also shown but is essentially indistinguishable from the case  $Da = 1 \times 10^{-2}$  and  $\psi = 0$  (dashed line). Note that in these plots  $\psi$  is only set to zero in the reaction term, not in the rest of the equations.

a current of  $I = 0$ , as found in [3] for the initial conditions studied here.

### B. Weak Water Dissociation Current

The reaction current spike at large bias voltage, as seen in the experimental data and numerical solutions of Figs. 2 to 5, correspond to incremental currents due to water dissociation. We estimate this reaction current spike here for weak reactions. The solution will apply for long scans so that the system is quasisteady and we can take  $\bar{\beta}$  to be a constant. Here the governing equations can be broken up into inner and outer solutions for large  $\chi$ . Further, from the expected parameter values the reaction is small relative to ion transport, and we can seek an asymptotic solution for  $\delta = Da \ll 1$ . We will also require  $\bar{m} \ll 1$  separately so that the equilibrium concentration is small.

#### 1. Inner region

For large  $\chi$  we can define an “inner” region, where the reaction is the strongest, that is of the order  $\chi^{-1}$ . We argue, using insight from the numerics, that the salt  $C_b^{(\pm)}$  has been swept away from this region and that to the leading order the positive ions are on the left-hand and negative ions on the right-hand membrane. Here we rescale as  $x = \eta/\chi$ , and ignore

time for large  $\chi$ . The steady equations for the inner region are

$$\frac{\partial^2 \phi'}{\partial \eta^2} = -(C_a^{(+)} - C_a^{(-)} + \Sigma), \quad (28)$$

for the potential, and

$$\alpha_a^{(+)} \frac{\partial}{\partial \eta} \left( \psi C_a^{(+)} \left( \chi \frac{\partial \phi'}{\partial \eta} + \bar{\beta}(0) \right) + \chi \frac{\partial C_a^{(+)}}{\partial \eta} \right) = -\delta R, \quad (29)$$

$$\alpha_a^{(-)} \frac{\partial}{\partial \eta} \left( -\psi C_a^{(-)} \left( \chi \frac{\partial \phi'}{\partial \eta} + \bar{\beta}(0) \right) + \chi \frac{\partial C_a^{(-)}}{\partial \eta} \right) = -\delta R, \quad (30)$$

for the ions created from water dissociation. Here  $R$  is the reaction defined as

$$R = \frac{1}{\chi} \left( \frac{1}{\bar{\epsilon}_r} + \psi |\phi'_\eta \chi + \bar{\beta}| - \frac{C_a^{(+)} C_a^{(-)}}{\bar{\epsilon}_r \bar{m}} \right). \quad (31)$$

Since the inner region is at quasi-steady-state, the following boundary conditions for the concentration are appropriate:  $C_a^{(+)}(-\infty) = 1$ ,  $C_a^{(-)}(-\infty) = 0$ ,  $C_a^{(+)}(\infty) = 0$ , and  $C_a^{(-)}(\infty) = \Sigma_2$ , which comes from the equilibrium result  $\rho^e = -\bar{\Sigma}$  and  $\phi'_{\eta\eta} = 0$  far from the junction.

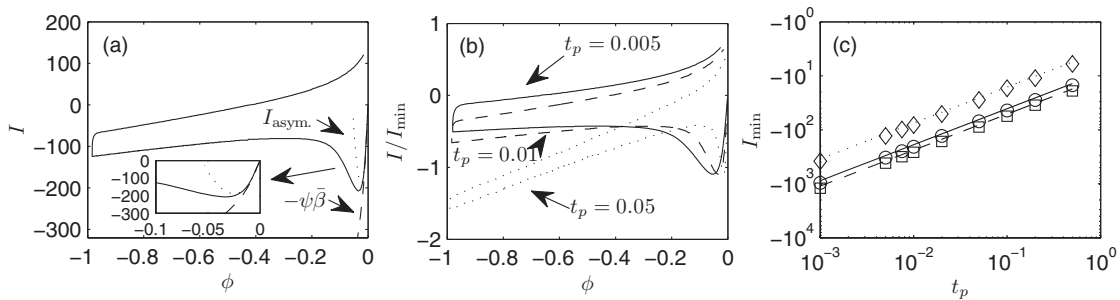


FIG. 5. Comparisons between the asymptotic and numerical solution. (a) Current vs potential curve showing the numerical solution (solid line) and the asymptotic solution (dotted line) for  $t_p = 0.01$ . The insert is a magnification of the region surrounding the minimum point. (b) Current scaled by the asymptotic minimum against potential. (c) Minimum current as a function of  $t_p$  with lines corresponding to the asymptotic solution and markers the numerical solution. The solid line (circle markers) corresponds to  $\chi = 5$  and  $\psi = 5 \times 10^3$ , the dotted line (diamond markers) to  $\chi = 20$  and  $\psi = 5 \times 10^3$ , and the dashed line (square markers) to  $\chi = 5$  and  $\psi = 10 \times 10^3$ . Here  $\bar{\beta} = (2t/t_p)$  ( $0 \leq t \leq t_p/2$ ),  $\bar{\beta} = 1 - (t - t_p/2)/(t_p - t_p/2)$  ( $t_p/2 \leq t \leq t_p$ ),  $\alpha_a^{(+)} = 3$ ,  $\alpha_a^{(-)} = 2$ ,  $\bar{m} = 1 \times 10^{-6}$ ,  $Da = 1 \times 10^{-2}$ ,  $\bar{\epsilon} = 1 \times 10^{-2}$ , and  $\bar{\Sigma}_2 = 1$ .

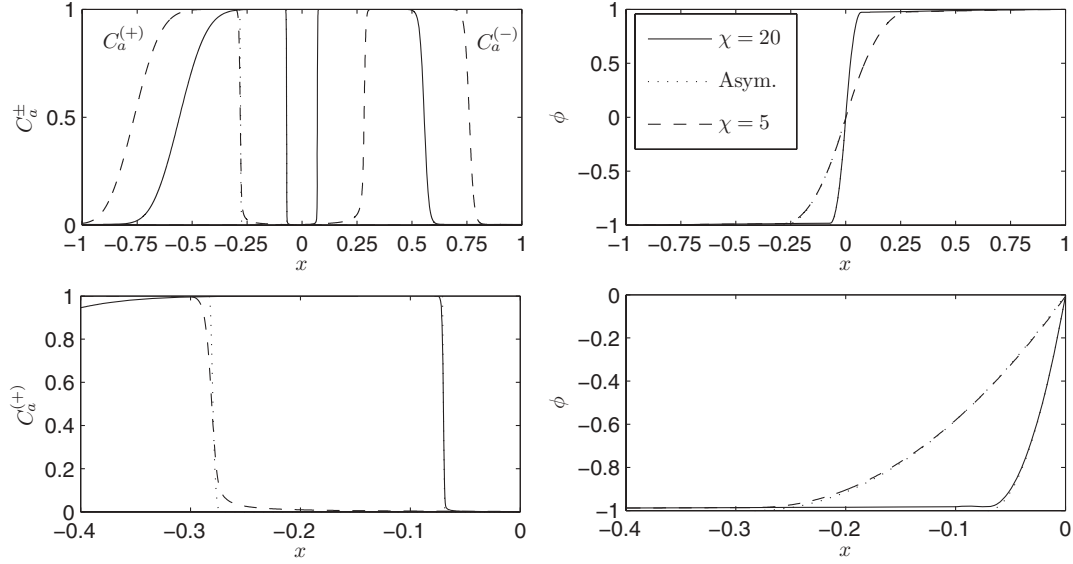


FIG. 6. Potential and concentration  $C_a^{(+)}$  comparing the numerical with the asymptotic solutions. The bottom panels are magnifications of the top panels showing asymptotic solutions (dotted lines) and the location of the Debye layer. Here  $\bar{m} = 1 \times 10^{-6}$ ,  $\epsilon = 1 \times 10^{-2}$ ,  $\bar{\beta} = 1$ ,  $\bar{\Sigma}_2 = 1$ ,  $\text{Da} = 1 \times 10^{-2}$ , and  $\psi = 5 \times 10^3$ .

Expressing Eqs. (29) and (30) in terms of ion fluxes and integrating from  $a$  to  $b$  yields the following:

$$[J_a^{(+)}]_a^b = [J_a^{(-)}]_a^b = -2\delta \int_a^b R d\eta. \quad (32)$$

Also, by subtracting Eqs. (29) and (30) we find that the current  $I$  is constant.

For  $\delta \ll 1$  we expand the above equations in powers of  $\delta$ ;  $\phi' = \phi'_0 + \delta\phi'_1 + \dots$  and similarly for the other variables. To the leading order the reaction is negligible and the flux of ions is constant in space, which is only possible if  $J_{a0}^{(-)} = J_{a0}^{(+)} = 0$ . This implies that an equilibrium has been established with an ion free region near the junction and electroneutrality in the rest of the membrane. Integrating Eqs. (29) and (30) with the boundary conditions at the ends of the domain, the concentration has a Boltzmann distribution. Inserting this solution into the equation for the potential, and converting back to  $x$  and  $\phi$ :

$$C_{a0}^{(+)} = \exp(-\psi(\phi_0 + \bar{\beta})), \quad (33)$$

$$C_{a0}^{(-)} = \bar{\Sigma}_2 \exp(\psi(\phi_0 - \bar{\beta})), \quad (34)$$

$$\phi_{0xx} = -\chi^2(C_{a0}^{(+)} - C_{a0}^{(-)} + \bar{\Sigma}(x)). \quad (35)$$

We can simplify Eq. (35) by separating the left-hand and right-hand membranes and matching the solutions at the junction with the conditions:  $\phi_0(0^-) = \phi_0(0^+) = \phi_j$  and  $\phi_{0x}(0^-) = \phi_{0x}(0^+)$ . Considering the region  $-1 \leq x \leq 0$  first, (35) is integrable [19,20] and we can reduce the order by multiplying both sides by  $d\phi/dx$  and integrating to get

$$\frac{d\phi}{dx} = \sqrt{2\chi^2\psi^{-1}\{(\bar{\beta} + \phi)\psi - 1 + \exp[-\psi(\phi + \bar{\beta})]\}^{1/2}}. \quad (36)$$

In deriving this equation the constant of integration was determined using the boundary condition  $\phi_0(-1) = -\bar{\beta}$ . Evaluating

this equation at  $x = 0$ , the magnitude of the electric field is  $d\phi/dx = \sqrt{2\chi^2(\bar{\beta} + \phi_j)}$ . Integrating this equation again

$$x = \frac{1}{\sqrt{2\chi^2\psi^{-1}}} \int_0^\phi \frac{dy}{\{(\bar{\beta} + y)\psi - 1 + \exp[-\psi(y + \bar{\beta})]\}^{1/2}}. \quad (37)$$

For large  $\psi$  the exponential is small in the ion free region, and we can approximate the integral near  $x = 0$  as

$$\phi = -\bar{\beta} + \left( (\bar{\beta} + \phi_j)^{1/2} + \sqrt{\frac{\chi^2}{2}} x \right)^2, \quad (38)$$

which is valid from  $x = 0$  to  $x \approx \lambda_L$ , the thickness of the ion free region. Similarly, in the region  $0 \leq x \leq \lambda_R$  the potential is

$$\phi = \bar{\beta} - \left( (\bar{\beta} - \phi_j)^{1/2} - \sqrt{\frac{\chi^2\bar{\Sigma}_2}{2}} x \right)^2. \quad (39)$$

From the jump condition for the electric field at the interface the potential at the junction is  $\phi_j = \beta(\bar{\Sigma}_2 - 1)/(1 + \bar{\Sigma}_2)$ .

Applying Eqs. (38) and (39) at  $\lambda_L$  and  $\lambda_R$ , respectively, the thickness of the polarized layers as a function of applied voltage and surface charge density in dimensionless form is

$$\lambda_L = \frac{2}{\chi} \sqrt{\bar{\beta} \frac{\bar{\Sigma}_2}{1 + \bar{\Sigma}_2}}, \quad \lambda_R = \frac{2}{\chi} \sqrt{\bar{\beta} \frac{\bar{\Sigma}_2^{-1}}{1 + \bar{\Sigma}_2}}, \quad (40)$$

$$\lambda = \lambda_L + \lambda_R = \frac{2}{\chi} \sqrt{\bar{\beta} \frac{1 + \bar{\Sigma}_2}{\bar{\Sigma}_2}}. \quad (41)$$

This estimate of the thickness of the polarized region without mobile ions is consistent with classical bipolar membrane or p-n junction theories [5,6].

Representative solutions are displayed in Fig. 6, showing the potential  $\phi$ , concentration  $C_a^{(\pm)}$ , and the asymptotic result

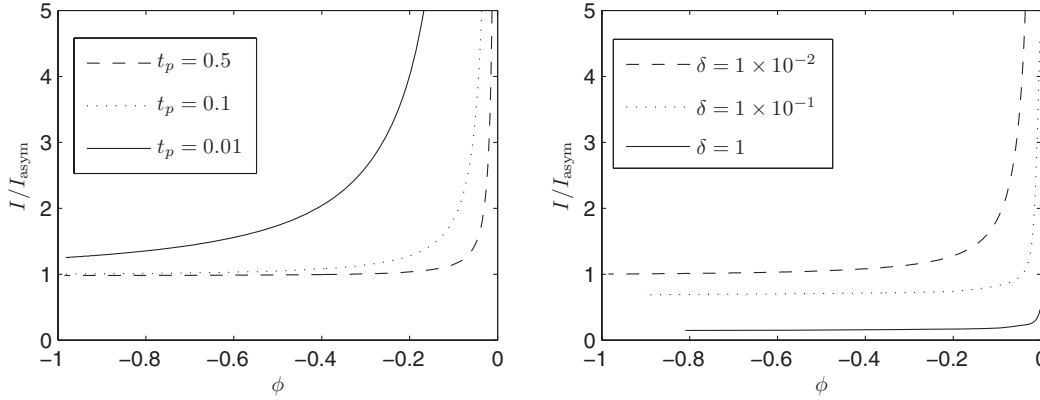


FIG. 7. Current, scaled by the asymptotic value found in Eq. (43), against voltage potential with the ramping up applied electric field,  $\beta = (2t/t_p)$  ( $0 \leq t \leq t_p/2$ ). Left-hand panel shows variations in  $t_p$  (for  $\delta = 1 \times 10^{-2}$ ), and the right-hand panel shows the results for variations in  $\delta$  (through changes in  $Da$  for  $t_p = 0.1$ ). In all cases  $\alpha_a^{(+)} = 3$ ,  $\alpha_a^{(-)} = 2$ ,  $\psi = 5 \times 10^2$ ,  $\bar{\epsilon}_r = 1 \times 10^{-2}$ ,  $\chi = 5$ ,  $\bar{m} = 1 \times 10^{-6}$ ,  $\bar{\beta} = 1$ , and  $\bar{\Sigma}_2 = 1$ .

for two different values of the inverse Debye length  $\chi$ . For  $\delta \ll 1$  the ion concentration given by (33) and (34) and the potential, given by (38), show excellent agreement with the numerical solutions.

Here the gradient of the potential peaks at the junction and decays to zero outside the ion free region of size  $\lambda$ . Since we have chosen parameter values such that the reaction is small relative to ion migration, this ion free region survives indefinitely. The width of this region is shown to decrease as  $\chi$  increases as found from the analytical result. Further from the ion free region a traveling wave propagates outward with positive ions moving to the left (negative membrane charge) and negative ions moving to the right (positive membrane charge). The concentration of species  $C_a^{(\pm)}$  upstream of the front is equal to the membrane charge, and the salt concentration ahead of the front is also equal to the membrane charge.

At the next order, the leading order potential is used to determine the ion flux as

$$J_{a1}^{(+)} = \int_{\lambda_L}^{\lambda_R} \left( \frac{1}{\bar{\epsilon}_r} - \frac{C_{a0}^{(+)} C_{a0}^{(-)}}{\bar{\epsilon}_r \bar{m}} \right) dx + \psi \int_{\lambda_L}^{\lambda_R} |\phi_{0x}| dx. \quad (42)$$

Since  $\psi \gg 1$ , the first term on the right-hand side is relatively small. The above integral can then be evaluated by noting that  $\phi(\lambda_L) = -\bar{\beta}$ ,  $\phi(\lambda_R) = \bar{\beta}$ , and  $d\phi/dx$  is always positive to get

$$-I_{\text{asym}} = J_a^{(+)} \approx 2\delta\psi\bar{\beta}. \quad (43)$$

This result shows that, at weak reaction, the  $I$ - $V$  spike due to water dissociation is Ohmic with a linear  $I$ - $V$  curve. This is verified in Fig. 7, which shows the numerically determined current relative to the asymptotic value of Eq. (43) for  $\bar{\beta}$  ramping up. In the figure the curves indicate that the asymptotic solution is approached for long scans such that system is in a quasi-steady-state and for sufficiently small values of  $\delta$ , indicating a slow reaction relative to ion migration. The water dissociation current for a p-n junction relative to the thermodynamic value (23) without charged membranes fully captures

the effect of ramping and bipolar membrane field enhancement on the yield,  $I_{\text{asym}}/I_{\text{therm}} = 2\delta/(\alpha_a^{(+)} + \alpha_a^{(-)})\sqrt{\bar{m} + \bar{m}\bar{\epsilon}_r\psi|\bar{\beta}|}$ .

## 2. Outer region: Traveling wave solution

The reaction current is controlled by the inner region, where the dissociation reaction occurs, and the reaction current also controls the propagation speeds of the proton and hydroxyl ion fronts observed in Fig. 6. From the numerical solution the wave speed looks roughly constant, but more so for the negative ion since the diffusivity is smaller. In the outer region far from the junction the ionic charge is in equilibrium with the membrane so that  $\rho^e \approx -\bar{\Sigma}$ , but positive ions are only present in the left-hand membrane, that is negatively charged and the opposite on the right-hand membrane. Considering only the region  $(-\infty, 0)$ , we seek a constant wave speed solution by shifting as  $x \rightarrow x - s^{(+)}t$  to move our reference frame with the traveling wave. Combining the ion equations we have the following condition on the current:

$$\frac{\partial \rho^e}{\partial t} = s^{(+)} \frac{\partial \rho^e}{\partial x} - \frac{\partial I}{\partial x}. \quad (44)$$

For  $\delta \ll 1$ , we can ignore the time derivative and integrate over the left-hand membrane to obtain the speed as

$$s^{(+)} = \frac{I}{\rho^e} \approx -J_a^{(+)} \sim -2\delta\psi\bar{\beta}, \quad (45)$$

since  $I = -J_a^{(+)}$  in the left-hand membrane. Similarly in the other membrane the front speed of the negative ion is  $s^{(-)} = J_a^{(-)}/\bar{\Sigma}_2$ .

In Fig. 8 we have plotted the concentration  $C_a^{(+)}$  on the left-hand side and in the shifted domain. For small  $Da$  (and thus small  $\delta$ ) the wave speed is roughly constant and the traveling-wave-like solution is appropriate. However for large  $\delta$  the current decreases in time as the front moves across the membrane and a constant wave speed solution does not exist. In panel (c) the front speed found numerically is plotted against the asymptotic result, showing good agreement in the limit of small  $\delta$ .

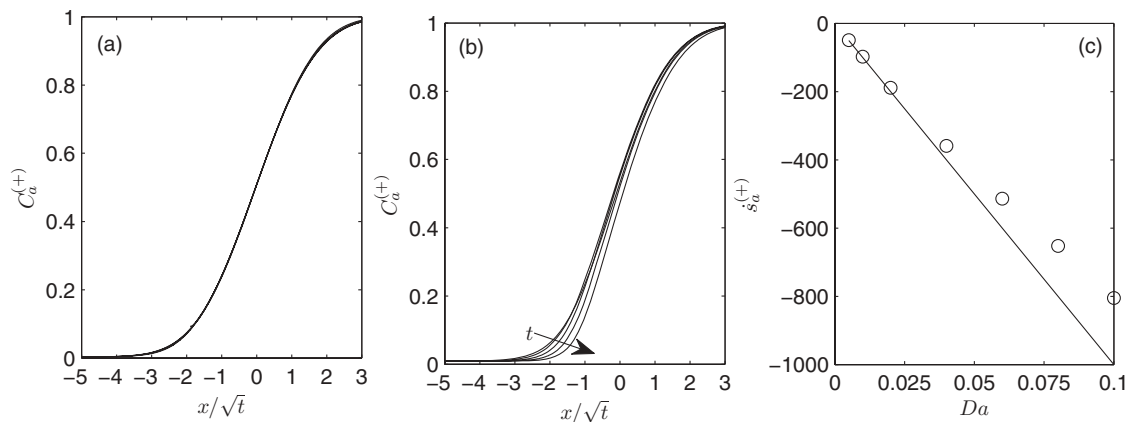


FIG. 8. (a-b) Front profiles at different times for (a)  $Da = 1 \times 10^{-2}$  and (b)  $1 \times 10^{-1}$ . (c) Front speed as a function of  $Da$  for the numerical (solid line) and asymptotic (circle markers) solutions. There are five lines evenly spaced between (a)  $t = 1.4 \times 10^{-3}$  to  $9.4 \times 10^{-3}$  and (b)  $t = 1.8 \times 10^{-4}$  to  $9.8 \times 10^{-4}$ . In all cases  $\psi = 5 \times 10^3$ ,  $\bar{\epsilon}_r = 1 \times 10^{-2}$ ,  $\chi = 20$ ,  $\bar{m} = 1 \times 10^{-6}$ ,  $\bar{\beta} = 1$ , and  $\bar{\Sigma}_2 = 1$ .

#### IV. CONCLUSION

We have quantified the nonequilibrium  $I$ - $V$  hysteresis of ion currents through the bipolar membrane, when forced by cyclic reverse voltage bias, due to incomplete ion depletion in the polarized layers of thickness  $\lambda$  at the junction. The hysteresis consists of a linear  $I$ - $V$  drop followed by a rise from the minimum current. The water dissociation current of  $I = -2\delta\psi\bar{\beta}$  is approached for long scans and small reaction relative to ion migration. For even longer scans or large biases, a reaction current spike with linear Ohmic  $I$ - $V$  dependence is found that signifies the onset of water dissociation. Inasmuch as reaction in the polarized region of a bipolar membrane is quite analogous to electron-transfer reactions at the Stern layer of an electrode—the electrode is electron selective and the electrolyte ion selective—we believe the same theory we have advanced here can also be used to analyze cyclic voltammetry of electron-transfer reactions at electrodes.

Several interesting features are already apparent from the current analysis. The decay at the minimum current in cyclic

voltammetry is traditionally described as a diffusive process with an inverse square root time dependence [21]. Our Eq. (26) shows that its scaling with respect to time is governed by the particular forcing function. The water-dissociation signature of (43), however, is approximately a shifted Ohmic line with an activation voltage, as is consistent with the measurements in Fig. 2(c) [4], where regime (3) is likely to be the shifted Ohmic line from regime (1).

#### ACKNOWLEDGMENTS

O.K.M. and R.V.C. would like to thank the Engineering and Physical Sciences Research Council (UK) for their support. O.K.M. would also like to acknowledge support received from the Faculty of Engineering of Imperial College to fund D.T.C. L.J.C. and H.-C.C. are supported by the AD&T initiative at the University of Notre Dame and by an NSF Grant No. CBET 1065652. This work was supported by a visiting Royal Academy of Engineering Distinguished Professorship awarded to H.-C.C., and was additionally supported by an EPSRC Mathematics Platform Grant No. EP/I019111/1.

- 
- [1] M. Samorski, G. Müller-Newen, and J. Büchs, *Biotechnol. Bioeng.* **92**, 61 (2005).
- [2] D. Kohlheyer, J. C. T. Eijkel, S. Schlautmann, A. van den Berg, and R. B. M. Schasfoort, *Anal. Chem.* **79**, 8190 (2007).
- [3] S. Mafe and P. Ramirez, *Acta Polym.* **48**, 234 (1997).
- [4] L.-J. Cheng and H.-C. Chang, *Biomicrofluidics* **5**, 046502 (2011).
- [5] P. Ramirez, H.-J. Rapp, S. Mafe, and B. Bauer, *J. Electroanal. Chem.* **375**, 101 (1994).
- [6] A. Alcaraz, P. Ramirez, S. Mafe, H. Holdik, and B. Bauer, *Polymer* **41**, 6627 (2000).
- [7] Y. Tanaka, *J. Membr. Sci.* **350**, 347 (2010).
- [8] R. Simons, *Desalination* **28**, 41 (1979).
- [9] R. Simons, *Electrochim. Acta* **29**, 151 (1984).
- [10] R. Simons, *Nature (London)* **280**, 824 (1979).
- [11] R. Simons, *Electrochim. Acta* **30**, 275 (1985).
- [12] V. I. Zabolotskii, S. V. Utin, K. A. Lebedev, P. A. Vasilenko, and N. V. Shel'deshov, *Russ. J. Electrochem.* **48**, 767 (2012).
- [13] D. Coelho, M. Shapiro, J. F. Thovet, and P. M. Adler, *J. Colloid Interface Sci.* **181**, 169 (1996).
- [14] H.-C. Chang and L. Y. Yeo, *Electrokinetically Driven Microfluidics and Nanofluidics* (Cambridge University Press, Cambridge, 2010).
- [15] J. A. Manzanares, W. D. Murphy, S. Mafe, and H. Reiss, *J. Phys. Chem.* **97**, 8524 (1993).
- [16] G. Yossifon, P. Mushenheim, Y.-C. Chang, and H.-C. Chang, *Phys. Rev. E* **79**, 046305 (2009).
- [17] A. Sokirko, P. Ramirez, J. A. Manzanares, and S. Mafe, *Ber. Bunsen-Ges. Phys. Chem.* **97**, 1040 (1993).
- [18] L.-J. Cheng and L. J. Guo, *ACS Nano* **3**, 575 (2009).
- [19] Y. Ben and H.-C. Chang, *J. Fluid Mech.* **461**, 229 (2002).
- [20] F. Flouraboué and H.-C. Chang, *Phys. Rev. E* **79**, 041404 (2009).
- [21] A. J. Bard and L. R. Faulkner, *Electrochemical Methods: Fundamentals and Applications* (Wiley, New York, 2001).